InSbAs Two-Dimensional Electron Gases as a Platform for Topological Superconductivity

Moehle, Christian M.; Ke, C.; Wang, Qingzhen; Xiao, Di; Karwal, Saurabh; Lodari, Mario; Van De Kerkhof, Vincent; Termaat, Ruben; Scappucci, Giordano; Goswami, Srijit

DOI
10.1021/acs.nanolett.1c03520

Publication date
2021

Document Version
Final published version

Published in
Nano Letters

NANO LETTERS

pubs.acs.org/NanoLett Letter

InSbAs Two-Dimensional Electron Gases as a Platform for Topological Superconductivity

Christian M. Moehle, Chung Ting Ke, Qingzhen Wang, Candice Thomas, Di Xiao, Saurabh Karwal, Mario Lodari, Vincent van de Kerkhof, Ruben Termaat, Geoffrey C. Gardner, Giordano Scappucci, Michael J. Manfra, and Srijit Goswami*

Cite This: *Nano Lett.* 2021, 21, 9990–9996 Read Online

ACCESS | Metrics & More | Article Recommendations | Supporting Information

ABSTRACT: Topological superconductivity can be engineered in semiconductors with strong spin−orbit interaction coupled to a superconductor. Experimental advances in this field have often been triggered by the development of new hybrid material systems. Among these, two-dimensional electron gases (2DEGs) are of particular interest due to their inherent design flexibility and scalability. Here, we discuss results on a 2D platform based on a ternary 2DEG (InSbAs) coupled to in situ grown aluminum. The spin−orbit coupling in these 2DEGs can be tuned with the As concentration, reaching values up to 400 meV Å, thus exceeding typical values measured in its binary constituents. In addition to a large Landé g-factor of ∼55 (comparable to that of InSb), we show that the clean superconductor−semiconductor interface leads to a hard induced superconducting gap. Using this new platform, we demonstrate the basic operation of phase-controllable Josephson junctions, superconducting islands, and quasi-1D systems, prototypical device geometries used to study Majorana zero modes.

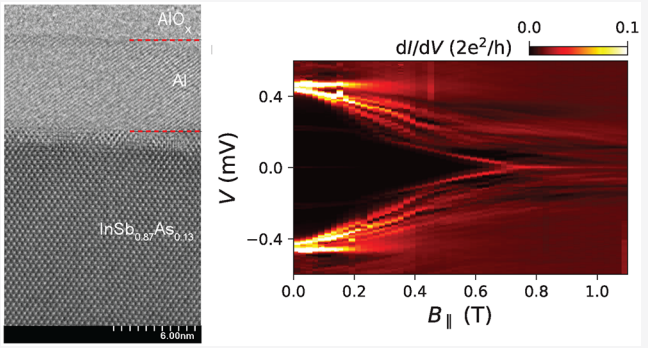

KEYWORDS: *two-dimensional electron gas, spin−orbit interaction, Josephson junctions, tunneling spectroscopy, topological superconductivity*

Topological phases of matter are currently a subject of intense research. Following early theoretical proposals,[1,2] materials with large spin−orbit interaction (such as InAs and InSb) coupled to superconductors have emerged as a promising platform to engineer topological superconductivity in the form of Majorana zero modes (MZMs). In this context, nanowires have been studied extensively over the years.[3−5] More recently, several efforts have been focused on engineering MZMs in two-dimensional electron gases (2DEGs). Not only do 2DEGs provide a scalable platform for future development of topological qubits, but their inherent flexibility allows for the realization of more complex devices. The versatility of the 2DEG platform can be seen in the variety of experiments performed on quasi-1D structures,[6] superconducting islands,[7] multiterminal Josephson junctions (JJs),[8] and phase-biased JJs,[9,10] all of which are promising architectures to create topological systems. Many of these studies have been performed on InAs 2DEGs, where it is possible to create a pristine interface between the superconductor aluminum (Al) and the 2DEG, allowing for a strong superconducting proximity effect.[11,12]

The InSb 2DEG is another appealing platform, primarily due to its significantly larger g-factor and spin−orbit coupling. Whereas the former allows the hybrid system to enter the topological regime at a lower magnetic field, the latter is crucial in determining the topological gap that protects the MZMs. These 2DEGs have recently been proximitized by ex situ superconductors;[13] however, there exist no reports of InSb-based hybrid systems with in situ grown superconductors. This could be related to the band offset at the InSb−Al interface, which (unlike InAs) prevents an efficient accumulation of charge carriers and hence induced superconductivity.[14] It would thus be ideal to have a material system with the desirable properties of both InAs and InSb.

In this work, we explore such a new hybrid material: ternary (InSbAs) 2DEGs coupled to in situ grown Al. Using magneto-transport experiments, we demonstrate a large g-factor (∼55) and exceptionally strong spin−orbit coupling exceeding the values of either InAs or InSb. In addition, the pristine semiconductor−superconductor interface leads to a hard

Received: September 10, 2021
Revised: October 26, 2021
Published: November 18, 2021

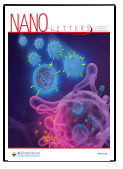

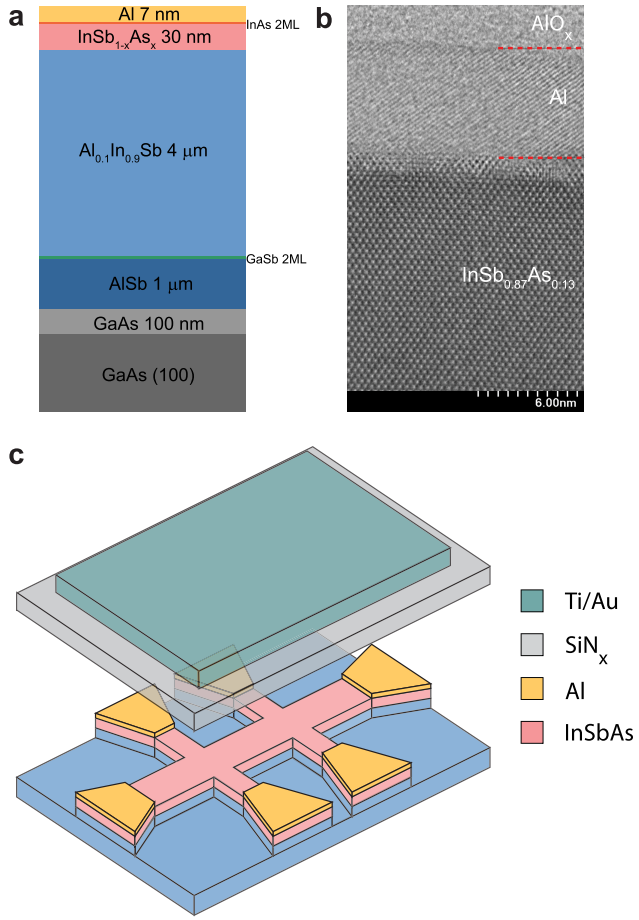

Figure 1. Hybrid Al/InSbAs heterostructures. (a) Layer stack of the Al/$InSb_{1-x}As_x$ hybrid heterostructures. (b) Bright-field scanning transmission electron micrograph of the Al-$InSb_{0.870}As_{0.130}$ interface along the [110] zone axis of the semiconductor. Red lines indicate the boundaries of the aluminum. (c) Schematic of a Hall bar that is used to extract the 2DEG properties.

induced superconducting gap that is revealed by spectroscopy measurements. Furthermore, using these ternary 2DEGs, we demonstrate the stable operation of prototypical devices studied in the context of MZMs: phase-controllable JJs, superconducting islands, and quasi-1D structures. Our results show that InSbAs/Al 2DEGs offer the combined advantages of their binary constituents and are therefore a promising platform to realize topological superconductivity.

$InSb_{1-x}As_x$ 2DEGs with varying As concentration, x, are grown by molecular beam epitaxy (MBE) on undoped, semi-insulating GaAs(100) substrates (see Figure 1a for a schematic of the layer stack). The growth starts with a 100 nm GaAs buffer layer, directly followed by a 1 μm thick AlSb nucleation layer[15] and a 4 μm thick $Al_{0.1}In_{0.9}Sb$ layer. The latter forms a closely matched pseudosubstrate for the $InSb_{1-x}As_x$ growth and the bottom barrier of the quantum well.[16] The As concentration in the $InSb_{1-x}As_x$ is controlled by the growth temperature and the As flux. In this study, heterostructures with x = 0, 0.053, 0.080, 0.130, 0.140, and 0.240 are grown. The semiconductor growth is terminated by the deposition of two monolayers (ML) of InAs, serving as a screening layer to prevent intermixing between the semiconductor structure and the superconducting Al layer.[17] After the semiconductor growth, the heterostructures are transferred under ultrahigh vacuum to a second MBE chamber to deposit 7 nm of Al, using methods described in ref 17. Figure 1b displays a bright-field scanning transmission electron micrograph focusing on the Al-$InSb_{1-x}As_x$ interface for x = 0.130. The interface appears sharp with a slight change of atomic contrast that is attributed to the relaxed InAs screening layer.[17] Further details about the growth process can be found in the Supporting Information (SI).

We characterize the semiconducting properties of the InSbAs 2DEGs by removing the Al in the active device area to fabricate Hall bars. After the Al removal, the 2DEG is etched in unwanted areas, followed by the deposition of a SiN_x dielectric layer. Lastly, a Ti/Au top gate is evaporated and used to control the electron density in the 2DEG (see Figure 1c for a schematic). We find peak mobilities of 20000−28000 cm^2/Vs (see SI for mobility−density curves and further details about the device fabrication).

To study the spin−orbit coupling in these 2DEGs, we measure the longitudinal conductivity, σ_{xx}, in perpendicular magnetic fields, $B_\perp$, at 300 mK using standard lock-in techniques. The simultaneously measured transversal Hall resistance allows us to deduce the density, n, in the 2DEG at every gate voltage, V_g. Figure 2a shows the magneto-conductivity correction, $\Delta\sigma_{xx}(B_\perp) = \sigma_{xx}(B_\perp) - \sigma_{xx}(0)$, at V_g = 0 V for x = 0, 0.053, 0.130, and 0.240, where the individual curves are offset for clarity. We observe clear weak antilocalization (WAL) peaks that are caused by the

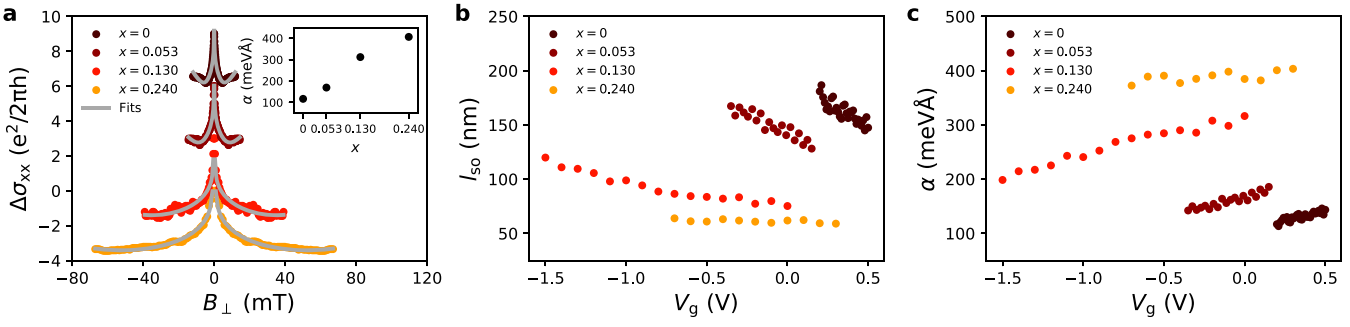

Figure 2. Large and tunable spin−orbit coupling. (a) Magneto-conductivity correction at V_g = 0 V for the different $InSb_{1-x}As_x$ 2DEGs. The x = 0 curve is measured at V_g = 0.2 V due to a high resistance at V_g = 0 V. The gray lines are ILP fits to the weak antilocalization data. In the inset, the extracted linear Rashba coefficient is plotted for the four As concentrations, showing a monotonic increase with increasing As concentration. For the higher As concentrations, α is 3−4 times larger than the value for pure InSb (x = 0). (b) Spin−orbit length plotted against V_g. (c) α as a function of V_g. l_{so} (α) decreases (increases) with increasing As concentration when compared at a fixed gate voltage.

https://doi.org/10.1021/acs.nanolett.1c03520
Nano Lett. 2021, 21, 9990−9996

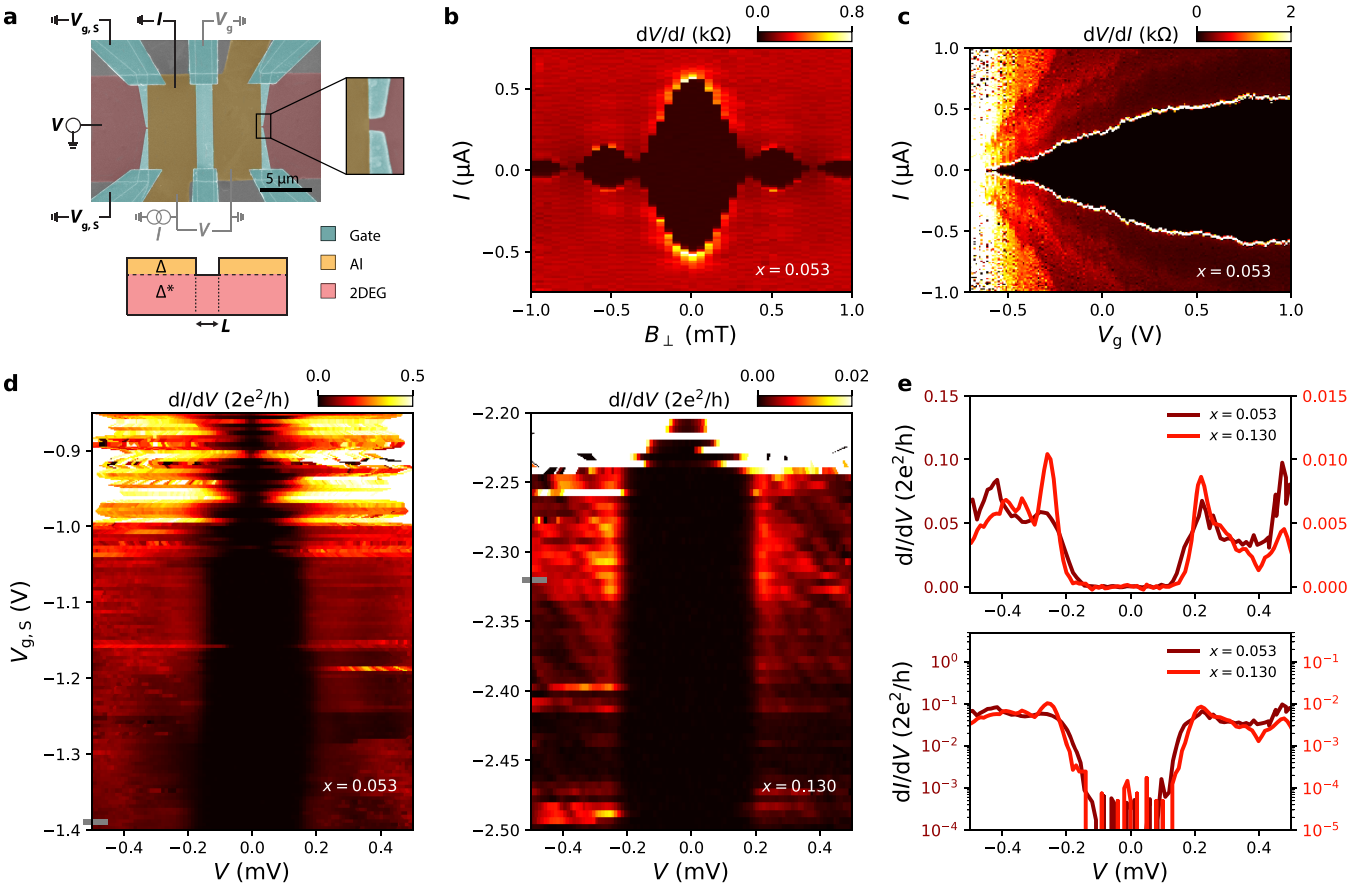

Figure 3. Hard induced superconducting gap. (a) False-colored SEM of a combined JJ and tunneling spectroscopy device. A cross-sectional schematic the JJ part is shown in the bottom. All devices have a fixed JJ length of $L \approx 150$ nm. (b) Differential resistance as a function of applied current bias and perpendicular magnetic field for the $x = 0.053$ JJ. The Fraunhofer interference pattern signifies a uniform current distribution in the JJ. (c) Differential resistance as a function of applied current bias and gate voltage for the same JJ, showing that the switching current, I_s, can be fully suppressed. (d) Differential conductance as a function of split-gate voltage and applied voltage bias for $x = 0.053$ and $x = 0.130$. The color scale has been saturated to increase the visibility of the tunneling regime. For both As concentrations, the induced superconducting gap is visible (region of suppressed conductance), stable over a large range in $V_{g,S}$. (e) Linecuts at the indicated positions (gray markers) on linear and logarithmic scale. The size of the induced gap is similar for both As concentrations. The in-gap conductance is suppressed by 2−3 orders of magnitude as compared to the out-of-gap conductance, indicating a hard induced gap.

suppression of coherent backscattering due to spin−orbit coupling. Since we expect the linear Rashba term to be the dominating spin−orbit contribution in these asymmetric quantum wells, we fit the WAL peaks with the Rashba-dominated Iordanskii, Lyanda-Geller, and Pikus (ILP) model[18,19] (gray curves in Figure 2a). This allows us to extract the spin−orbit length, $l_{so} = \sqrt{D\tau_{so}}$, where $D = v_F l_e/2$ is the diffusion constant. Here, τ_{so} is the spin−orbit scattering time, v_F the Fermi velocity, and l_e the mean free path. The linear Rashba parameter is given by $\alpha = \Delta_{so}/2k_F$, where $\Delta_{so} = \sqrt{2\hbar^2/\tau_{so}\tau_e}$ is the spin-split energy, k_F the Fermi wave vector, and τ_e the elastic scattering time.

As shown in Figure 2a, the ILP model fits the experimental data well. The resulting linear Rashba parameter for the four different As concentrations is plotted in the inset. It is striking that α increases monotonically with increasing As concentration. Compared to the value for pure InSb ($\alpha \approx 100$ meV Å), it is noteworthy that for the higher As concentrations, the linear Rashba parameter is 3−4 times larger (300−400 meV Å). We proceed by measuring WAL as a function of gate voltage (V_g) for the different As concentrations. In Figure 2b,c, we show l_{so} and α plotted against V_g (see SI for the same plots as a function of electron density). The trend of decreasing (increasing) l_{so} (α) with increasing As concentration persists also when compared at other gate voltages. We note, however, that specifically for $x = 0.240$, the spin−orbit coupling becomes so large that l_{so} is smaller than l_e. This might lead to inaccuracies in the extracted fit parameters as the ILP model is valid when l_e is the smallest length scale.

The systematic increase in spin−orbit coupling with As concentration can arise from a combination of several effects. First, band structure calculations of $InSb_{1-x}As_x$ show that the Rashba parameter is strongly influenced by the As concentration,[20,21] which has been observed in experiments on ternary nanowires.[22] Second, electric fields across the 2DEG can also influence the spin−orbit interaction. We note that even at $V_g = 0$ V, α increases monotonically with x, suggesting that the external electric field from the applied gate voltage is not the primary source of the enhancement. However, the internal field (generated at the 2DEG−gate dielectric interface) could be a strong function of the As concentration. We indeed observe that the nominal density in the 2DEG (density at $V_g = 0$ V) increases systematically with As concentration (see SI), indicating a stronger downward band bending at the dielectric−semiconductor interface, resulting in an increased

https://doi.org/10.1021/acs.nanolett.1c03520
Nano Lett. 2021, 21, 9990−9996

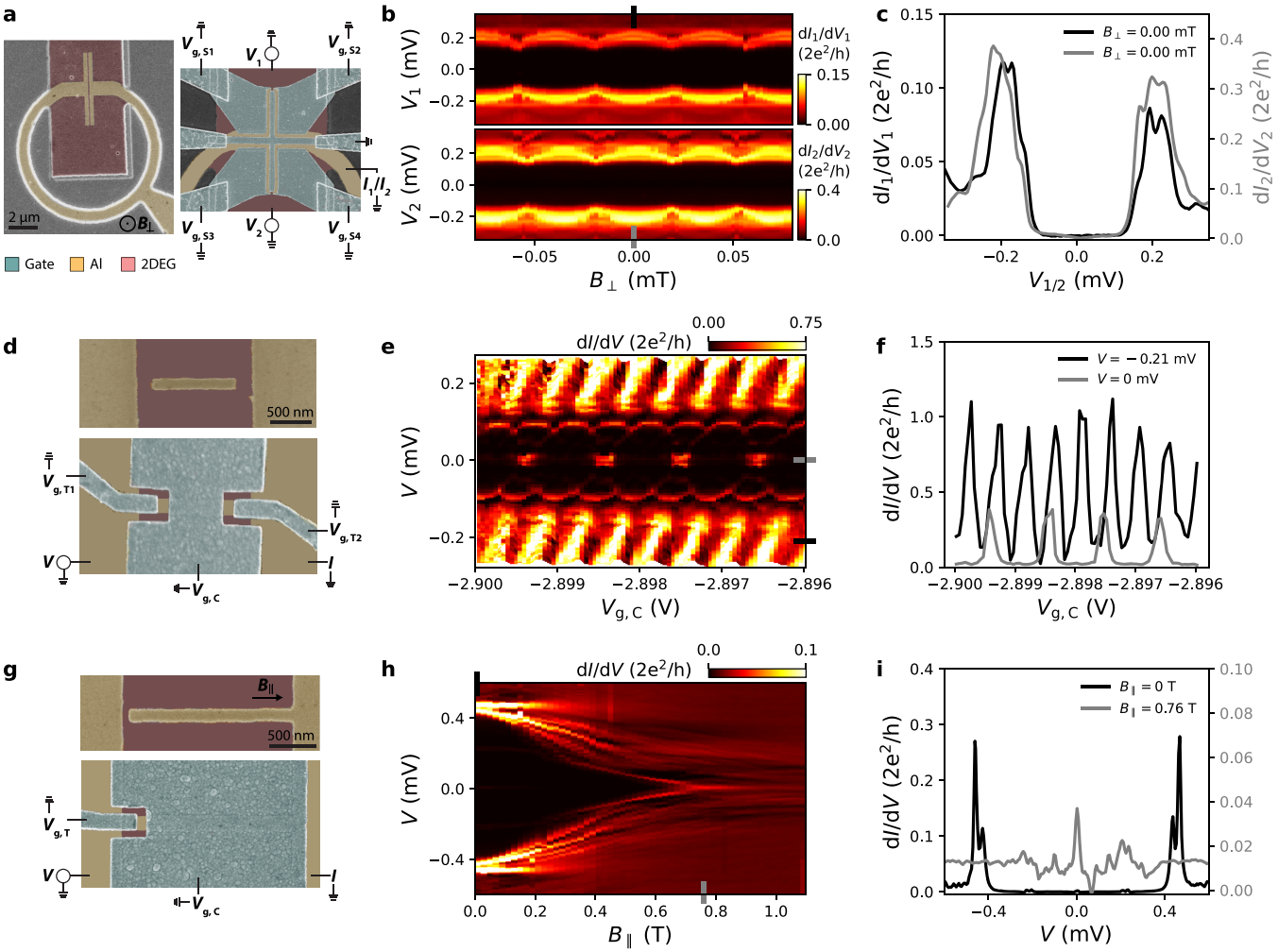

Figure 4. Prototypical Majorana devices. (a) False-colored SEMs of a phase-biased JJ before (left) and after (right) gate deposition. The split gates at the top and bottom edge of the JJ are used to perform tunneling spectroscopy at both ends of the JJ. This device is fabricated on a 2DEG with x = 0.080. (b) Differential conductance as a function of voltage bias applied to the top contact and perpendicular magnetic field while the bottom contact is floating (top panel). The bottom panel shows the tunneling spectroscopy map as a function of bottom voltage bias and perpendicular magnetic field (top contact floating). For both measurements, the split gates are fixed at $V_{g,S1}$ = −2.36 V, $V_{g,S2}$ = −1.36 V, and $V_{g,S3}$ = $V_{g,S4}$ = −1.48 V. (c) Linecuts from (b) at the indicated positions. (d) SEMs of a superconducting island before (top) and after (bottom) gate deposition, fabricated on a 2DEG with x = 0.140. The two tunnel gates are used to tune the transmission between the leads and the island. The central gate depletes the surrounding 2DEG and changes the charge occupancy of the island. (e) Differential conductance at fixed tunnel gate voltages ($V_{g,T1}$ = −2.157 V, $V_{g,T2}$ = −2.052 V) as a function of applied voltage bias and central gate voltage. 2e-periodic Coulomb oscillations are visible at V = 0 mV, and 1e-periodic Coulomb oscillations are visible at high biases. (f) Linecuts from (e) at the indicated positions. (g) SEMs of a quasi-1D grounded superconducting strip before (top) and after (bottom) gate deposition. The left gate is used to create a tunnel barrier between the bulk Al contact and the superconducting strip, and the central gate depletes the surrounding 2DEG. This device is fabricated on a 2DEG with x = 0.140. (h) Differential conductance at fixed gate voltages ($V_{g,T}$ = −3.96 V, $V_{g,C}$ = −4.40 V) as a function of applied voltage bias and parallel magnetic field. (i) Linecuts from (h) at the indicated positions.

electric field. While from these studies it is difficult to disentangle the effects of the bulk semiconductor from the interfaces, similar experiments on deep InSbAs quantum wells would shed more light on the origins of the enhanced spin−orbit interaction.

Having established strong spin−orbit coupling in $InSb_{1-x}As_x$ 2DEGs, we proceed by measuring the perpendicular g-factor, g^*. By comparing the temperature dependence of Shubnikov−de Haas oscillations for an odd−even filling factor couple, an expression for g^* can be obtained.[23] For x = 0, we find g^* = 47.8 ± 2.8. The same analysis is done for x = 0.130, where we obtain g^* = 54.6 ± 3.1 (see SI for details about the data analysis, as well as effective mass measurements for the two As concentrations). This shows that, in addition to strong spin−orbit coupling, InSbAs 2DEGs also possess a large g-factor that is comparable to the one of pure InSb.

Given that the semiconducting properties of InSbAs 2DEGs are favorable to realize topological phases, we now demonstrate that these 2DEGs also have excellent coupling to Al. To do so, we use devices as shown in the false-colored scanning electron micrograph (SEM) in Figure 3a. This device can either be operated as a gate-tunable JJ (gray circuit) or a spectroscopy device (black circuit) to measure the local density of states. All devices are measured at a temperature of 30 mK.

It is important to note that we do not see any induced superconductivity for pure InSb, presumably due to an unfavorable band alignment at the Al−InSb interface. In

https://doi.org/10.1021/acs.nanolett.1c03520
Nano Lett. 2021, 21, 9990−9996

stark contrast, all of the InSbAs 2DEGs (irrespective of As concentration) have excellent coupling to the superconductor, where all JJs display supercurrents and pronounced multiple Andreev reflections (see SI). In Figure 3b, we show a representative Fraunhofer interference pattern for the JJ with $x = 0.053$, where the black regions correspond to zero resistance. The size of the switching current, I_s, can be controlled by the gate voltage, as demonstrated in Figure 3c for the same As concentration. Upon lowering V_g, I_s shrinks, and correspondingly, the normal-state resistance of the JJ increases.

Clean and transparent interfaces are crucial for the realization of MZMs as they allow the proximitized semiconductor to obtain a hard induced superconducting gap with a vanishing in-gap density of states. It is therefore important to measure the density of states in the proximitized 2DEG directly. To this end, we operate the devices shown in Figure 3a as spectroscopy devices. We apply a voltage bias to the left normal contact and measure the current flowing through the Al lead, while energizing the split gates with a negative voltage, $V_{g,S}$, to create a barrier. In the tunneling regime, the measured conductance is proportional to the density of states in the proximitized 2DEG. In Figure 3d, we present tunneling spectroscopy maps for $x = 0.053$ and $x = 0.130$. In both measurements, we note the emergence of a region with suppressed conductance, reflecting the induced superconducting gap. The gaps persist over an extended range in $V_{g,S}$ with a slight dependence of the gap size on the out-of-gap conductance. In Figure 3e, we show two representative linecuts in the tunneling regime. We find that the size of the induced gap is similar for both As concentrations ($\Delta^* \approx 220$ μeV). Turning to the linecuts on the logarithmic scale and comparing the out-of-gap conductance with the in-gap conductance, we see that the in-gap conductance is suppressed by 2−3 orders of magnitude for both As concentrations. This confirms the excellent Al−2DEG interface.

Using the InSbAs/Al hybrid platform, we realize three prototypical device architectures used to study MZMs: phase-controllable JJs, superconducting islands, and quasi-1D superconducting strips. Figure 4a shows false-colored SEMs of a JJ embedded in a superconducting loop. A perpendicular magnetic field, $B_\perp$, penetrating through the loop can be used to tune the phase difference across the JJ. Split gates are positioned at the top and bottom edge of the JJ to perform tunneling spectroscopy at both ends of the phase-controllable JJ. In Figure 4b, we show spectroscopy maps at the top (top panel) and bottom (bottom panel) of the JJ, with representative linecuts shown in Figure 4c. In both cases, we observe a clear flux-dependent modulation of the gap, consistent with the phase modulation expected for Andreev-bound states. Such three-terminal devices are important to check for correlations between the two ends of the JJ when tuned into the topological regime.

A second approach to create MZMs is based on a floating narrow strip of superconductor, a superconducting island (see Figure 4d). Here, two tunnel gates are used to tune the transmission between the bulk Al contacts and the island. The central gate depletes the 2DEG in areas that are not covered with Al and changes the charge occupancy on the island. In Figure 4e, we show a differential conductance map at fixed tunnel gate voltages varying the applied voltage bias, V, and the central gate voltage, $V_{g,C}$. At $V = 0$ mV (see also gray linecut in Figure 4f), we observe Coulomb peaks that have twice the spacing compared to the Coulomb peaks at high biases (black linecut in Figure 4f). The Coulomb peaks at $V = 0$ mV reflect 2e-periodic Cooper pair transport through the superconducting island, while at high biases, quasiparticles with 1e charge are allowed to tunnel through the island.

Another strategy to study MZMs employs a grounded narrow strip of superconductor (see Figure 4g). The narrow gate is used to define a tunnel barrier between the bulk Al contact and the quasi-1D strip, and the central gate depletes the remaining exposed 2DEG. In Figure 4h, we present a tunneling spectroscopy map at fixed gate voltages as a function of applied voltage bias, V, and magnetic field, $B_\parallel$. $B_\parallel$ is oriented along the superconducting finger. Two representative linecuts are shown in Figure 4i. Whereas at $B_\parallel = 0$ T we observe a hard induced superconducting gap (note that the gap size is doubled due to the superconducting contact), a zero energy state emerges around $B_\parallel = 0.7$ T. While these results are promising, further experiments are required to comment on the origin of these states.

In conclusion, we have shown that InSbAs 2DEGs offer the combined advantages of the more commonly studied binary materials. In addition to a large g-factor, they have excellent coupling to in situ grown aluminum. Furthermore, the spin−orbit coupling in these ternary 2DEGs is significantly stronger than in either InAs or InSb. Using this hybrid system, we realize distinct device architectures that can be used to study topological superconductivity.

■ ASSOCIATED CONTENT

Supporting Information

The Supporting Information is available free of charge at https://pubs.acs.org/doi/10.1021/acs.nanolett.1c03520.

Wafer growth and characterization, device fabrication, mobility and density measurements, effect of electron density on spin−orbit coupling, effective mass and g-factor measurements, multiple Andreev reflections measurements (PDF)

■ AUTHOR INFORMATION

Corresponding Author

Srijit Goswami − *QuTech and Kavli Institute of Nanoscience, Delft University of Technology, 2600 GA Delft, The Netherlands;* orcid.org/0000-0002-9095-4363; Email: s.goswami@tudelft.nl

Authors

Christian M. Moehle − *QuTech and Kavli Institute of Nanoscience, Delft University of Technology, 2600 GA Delft, The Netherlands;* orcid.org/0000-0002-6094-3663

Chung Ting Ke − *QuTech and Kavli Institute of Nanoscience, Delft University of Technology, 2600 GA Delft, The Netherlands*

Qingzhen Wang − *QuTech and Kavli Institute of Nanoscience, Delft University of Technology, 2600 GA Delft, The Netherlands*

Candice Thomas − *Department of Physics and Astronomy and Birck Nanotechnology Center, Purdue University, West Lafayette, Indiana 47907, United States*

Di Xiao − *Department of Physics and Astronomy and Birck Nanotechnology Center, Purdue University, West Lafayette, Indiana 47907, United States*

https://doi.org/10.1021/acs.nanolett.1c03520
Nano Lett. 2021, 21, 9990−9996

Saurabh Karwal − *QuTech and Netherlands Organization for Applied Scientific Research (TNO), 2628 CK Delft, The Netherlands*
Mario Lodari − *QuTech and Kavli Institute of Nanoscience, Delft University of Technology, 2600 GA Delft, The Netherlands*
Vincent van de Kerkhof − *QuTech and Kavli Institute of Nanoscience, Delft University of Technology, 2600 GA Delft, The Netherlands*
Ruben Termaat − *QuTech and Kavli Institute of Nanoscience, Delft University of Technology, 2600 GA Delft, The Netherlands*
Geoffrey C. Gardner − *Microsoft Quantum Purdue, Purdue University, West Lafayette, Indiana 47907, United States*
Giordano Scappucci − *QuTech and Kavli Institute of Nanoscience, Delft University of Technology, 2600 GA Delft, The Netherlands;* orcid.org/0000-0003-2512-0079
Michael J. Manfra − *Department of Physics and Astronomy, Birck Nanotechnology Center, Microsoft Quantum Purdue, School of Electrical and Computer Engineering, and School of Materials Engineering, Purdue University, West Lafayette, Indiana 47907, United States*

Complete contact information is available at: https://pubs.acs.org/10.1021/acs.nanolett.1c03520

Author Contributions

C.M.M. and C.T.K contributed equally, fabricated and measured the devices together with Q.W., S.K., V.vdK., and R.T. The MBE growth of the semiconductor heterostructures and the characterization of the materials was performed by C.T., D.X., and G.C.G. under the supervision of M.J.M. The effective mass and g-factor measurements were provided by M.L. and G.S. The manuscript was written by C.M.M., C.T.K., and S.G., with input from all co-authors. S.G. supervised the experimental work in Delft.

Notes

The authors declare no competing financial interest.
Raw data and analysis scripts for all presented figures are available at the 4TU.ResearchData repository, DOI: https://doi.org/10.4121/14565228.

■ ACKNOWLEDGMENTS

We thank Michael Wimmer and Michal P. Nowak for useful discussions. Moreover, we would like to thank J.H. Dycus, M.E. Salmon, and R.E. Daniel from Eurofins EAG Materials Science for the TEM studies. The research at Delft was supported by the Dutch National Science Foundation (NWO), the Early Research Programme of The Netherlands Organisation for Applied Scientific Research (TNO), and a TKI grant of the Dutch Topsectoren Program. The work at Purdue was funded by Microsoft Quantum.

■ REFERENCES

(1) Lutchyn, R. M.; Sau, J. D.; Das Sarma, S. Majorana Fermions and a Topological Phase Transition in Semiconductor-Superconductor Heterostructures. *Phys. Rev. Lett.* **2010**, *105*, 077001.
(2) Oreg, Y.; Refael, G.; von Oppen, F. Helical Liquids and Majorana Bound States in Quantum Wires. *Phys. Rev. Lett.* **2010**, *105*, 177002.
(3) Aguado, R. Majorana quasiparticles in condensed matter. *La Rivista del Nuovo Cimento* **2017**, *40*, 523−593.
(4) Lutchyn, R. M.; Bakkers, E. P. A. M.; Kouwenhoven, L. P.; Krogstrup, P.; Marcus, C. M.; Oreg, Y. Majorana zero modes in superconductor−semiconductor heterostructures. *Nature Reviews Materials* **2018**, *3*, 52−68.
(5) Prada, E.; San-Jose, P.; de Moor, M. W. A.; Geresdi, A.; Lee, E. J. H.; Klinovaja, J.; Loss, D.; Nygård, J.; Aguado, R.; Kouwenhoven, L. P. From Andreev to Majorana bound states in hybrid superconductor-semiconductor nanowires. *Nature Reviews Physics* **2020**, *2*, 575−594.
(6) Nichele, F.; Drachmann, A. C. C.; Whiticar, A. M.; O'Farrell, E. C. T.; Suominen, H. J.; Fornieri, A.; Wang, T.; Gardner, G. C.; Thomas, C.; Hatke, A. T.; Krogstrup, P.; Manfra, M. J.; Flensberg, K.; Marcus, C. M. Scaling of Majorana Zero-Bias Conductance Peaks. *Phys. Rev. Lett.* **2017**, *119*, 136803.
(7) O'Farrell, E. C. T.; Drachmann, A. C. C.; Hell, M.; Fornieri, A.; Whiticar, A. M.; Hansen, E. B.; Gronin, S.; Gardner, G. C.; Thomas, C.; Manfra, M. J.; Flensberg, K.; Marcus, C. M.; Nichele, F. Hybridization of Subgap States in One-Dimensional Superconductor-Semiconductor Coulomb Islands. *Phys. Rev. Lett.* **2018**, *121*, 256803.
(8) Pankratova, N.; Lee, H.; Kuzmin, R.; Wickramasinghe, K.; Mayer, W.; Yuan, J.; Vavilov, M. G.; Shabani, J.; Manucharyan, V. E. Multiterminal Josephson Effect. *Phys. Rev. X* **2020**, *10*, 031051.
(9) Fornieri, A.; Whiticar, A. M.; Setiawan, F.; Portolés, E.; Drachmann, A. C. C.; Keselman, A.; Gronin, S.; Thomas, C.; Wang, T.; Kallaher, R.; Gardner, G. C.; Berg, E.; Manfra, M. J.; Stern, A.; Marcus, C. M.; Nichele, F. Evidence of topological superconductivity in planar Josephson junctions. *Nature* **2019**, *569*, 89−92.
(10) Ren, H.; Pientka, F.; Hart, S.; Pierce, A. T.; Kosowsky, M.; Lunczer, L.; Schlereth, R.; Scharf, B.; Hankiewicz, E. M.; Molenkamp, L. W.; Halperin, B. I.; Yacoby, A. Topological superconductivity in a phase-controlled Josephson junction. *Nature* **2019**, *569*, 93−98.
(11) Shabani, J.; Kjaergaard, M.; Suominen, H. J.; Kim, Y.; Nichele, F.; Pakrouski, K.; Stankevic, T.; Lutchyn, R. M.; Krogstrup, P.; Feidenhans'l, R.; Kraemer, S.; Nayak, C.; Troyer, M.; Marcus, C. M.; Palmstrøm, C. J. Two-dimensional epitaxial superconductor-semiconductor heterostructures: A platform for topological superconducting networks. *Phys. Rev. B: Condens. Matter Mater. Phys.* **2016**, *93*, 155402.
(12) Kjaergaard, M.; Nichele, F.; Suominen, H. J.; Nowak, M. P.; Wimmer, M.; Akhmerov, A. R.; Folk, J. A.; Flensberg, K.; Shabani, J.; Palmstrøm, C. J.; Marcus, C. M. Quantized conductance doubling and hard gap in a two-dimensional semiconductor−superconductor heterostructure. *Nat. Commun.* **2016**, *7*, 12841.
(13) Ke, C. T.; Moehle, C. M.; de Vries, F. K.; Thomas, C.; Metti, S.; Guinn, C. R.; Kallaher, R.; Lodari, M.; Scappucci, G.; Wang, T.; Diaz, R. E.; Gardner, G. C.; Manfra, M. J.; Goswami, S. Ballistic superconductivity and tunable π-junctions in InSb quantum wells. *Nat. Commun.* **2019**, *10*, 3764.
(14) Schuwalow, S.; Schröter, N. B. M.; Gukelberger, J.; Thomas, C.; Strocov, V.; Gamble, J.; Chikina, A.; Caputo, M.; Krieger, J.; Gardner, G. C.; Troyer, M.; Aeppli, G.; Manfra, M. J.; Krogstrup, P. Band Structure Extraction at Hybrid Narrow-Gap Semiconductor-Metal Interfaces. *Advanced Science* **2021**, *8*, 2003087.
(15) Goldammer, K.; Chung, S.; Liu, W.; Santos, M.; Hicks, J.; Raymond, S.; Murphy, S. High-mobility electron systems in remotely-doped InSb quantum wells. *J. Cryst. Growth* **1999**, *201−202*, 753−756.
(16) Lehner, C. A.; Tschirky, T.; Ihn, T.; Dietsche, W.; Keller, J.; Fält, S.; Wegscheider, W. Limiting scattering processes in high-mobility InSb quantum wells grown on GaSb buffer systems. *Phys. Rev. Materials* **2018**, *2*, 054601.
(17) Thomas, C.; Diaz, R. E.; Dycus, J. H.; Salmon, M. E.; Daniel, R. E.; Wang, T.; Gardner, G. C.; Manfra, M. J. Toward durable Al-InSb hybrid heterostructures via epitaxy of 2 ML interfacial InAs screening layers. *Phys. Rev. Materials* **2019**, *3*, 124202.
(18) Iordanskii, S. V.; Lyanda-Geller, Y. B.; Pikus, G. E. Weak-Localization in Quantum-Wells With Spin-Orbit Interaction. *Zh. Eksp. Teor. Fiz.* **1994**, *60*, 199−203.
(19) Knap, W.; Skierbiszewski, C.; Zduniak, A.; Litwin-Staszewska, E.; Bertho, D.; Kobbi, F.; Robert, J. L.; Pikus, G. E.; Pikus, F. G.; Iordanskii, S. V.; Mosser, V.; Zekentes, K.; Lyanda-Geller, Y. B. Weak

antilocalization and spin precession in quantum wells. *Phys. Rev. B: Condens. Matter Mater. Phys.* **1996**, *53*, 3912−3924.
(20) Winkler, G. W.; Wu, Q.; Troyer, M.; Krogstrup, P.; Soluyanov, A. A. Topological Phases in $InAs_{1-x}Sb_x$: From Novel Topological Semimetal to Majorana Wire. *Phys. Rev. Lett.* **2016**, *117*, 076403.
(21) Mayer, W.; Schiela, W. F.; Yuan, J.; Hatefipour, M.; Sarney, W. L.; Svensson, S. P.; Leff, A. C.; Campos, T.; Wickramasinghe, K. S.; Dartiailh, M. C.; Žutić, I.; Shabani, J. Superconducting Proximity Effect in InAsSb Surface Quantum Wells with In Situ Al Contacts. *ACS Applied Electronic Materials* **2020**, *2*, 2351−2356.
(22) Sestoft, J. E.; Kanne, T.; Gejl, A. N.; von Soosten, M.; Yodh, J. S.; Sherman, D.; Tarasinski, B.; Wimmer, M.; Johnson, E.; Deng, M.; Nygård, J.; Jespersen, T. S.; Marcus, C. M.; Krogstrup, P. Engineering hybrid epitaxial InAsSb/Al nanowires for stronger topological protection. *Phys. Rev. Materials* **2018**, *2*, 044202.
(23) Drichko, I. L.; Dmitriev, A. A.; Malysh, V. A.; Smirnov, I. Y.; von Känel, H.; Kummer, M.; Chrastina, D.; Isella, G. Effective g factor of 2D holes in strained Ge quantum wells. *J. Appl. Phys.* **2018**, *123*, 165703.

https://doi.org/10.1021/acs.nanolett.1c03520
Nano Lett. 2021, 21, 9990−9996